

## Enhancing synchronization by optimal correlated noise

Sherwood Martineau, Tim Saffold, Timothy T. Chang, and Henrik Ronellenfitsch\*  
*Physics Department, Williams College, 33 Lab Campus Drive, Williamstown, MA 01267, U.S.A.*  
 (Dated: March 2, 2022)

From the flashes of fireflies to Josephson junctions and power infrastructure, networks of coupled phase oscillators provide a powerful framework to describe synchronization phenomena in many natural and engineered systems. Most real-world networks are under the influence of noisy, random inputs, potentially inhibiting synchronization. While noise is unavoidable, here we show that there exist optimal noise patterns which minimize desynchronizing effects and even enhance order. Specifically, using analytical arguments we show that in the case of a two-oscillator model, there exists a sharp transition from a regime where the optimal synchrony-enhancing noise is perfectly anti-correlated, to one where the optimal noise is correlated. More generally, we then use numerical optimization methods to demonstrate that there exist anti-correlated noise patterns that optimally enhance synchronization in large complex oscillator networks. Our results may have implications in networks such as power grids and neuronal networks, which are subject to significant amounts of correlated input noise.

The occurrence of noise is unavoidable in networks and systems at all scales [1], from biological examples [2] such as neurons in the auditory and visual pathways [3–5], neural information processing [6, 7] to mechanical oscillators [8] and fluctuating inputs affecting the stability of power grids [9–11]. Synchronization of the underlying network of nonlinear phase oscillators is a paradigm employed to understand such physical and biological networks [12, 13]. Fluctuations are generally seen as undesirable and significant efforts have been made to understand and prevent their detrimental effects on network synchronization [14–19]. Optimization methods have been successfully employed to improve synchrony with and without noise, in particular by adjusting the weighted network topology [17, 20–28]. Similar techniques have also been effective for other types of networks and objectives such as efficient transport [29–35]. There has been recent interest in the possibility that noise may be leveraged to enhance synchronization [36–43]. Specifically, it was found that the degree to which input noise is correlated may have a significant influence on its ability to aid in or prevent network synchrony [36].

Based on the widely used Kuramoto model [44, 45], here we study the optimal patterns of input noise correlations that enhance synchronization in networks of oscillators. Using analytic arguments we find that in the simple case of two coupled oscillators in the phase-drift regime as studied in Ref. [36], the optimal synchrony-enhancing noise undergoes a transition from perfect anti-correlation to perfect correlation as the total noise strength is increased. We then numerically study generic complex networks near phase-locked fixed points and show that the optimal pattern of synchrony-enhancing noise retains essential characteristics seen in the two-oscillator case. The optimal noise we uncover is strongly linked to the network topology. In complex networks, the optimal noise correlations show characteristic clustering, separating the

network into regions that benefit from receiving uncorrelated inputs. We now proceed to analytically study the tractable case of two connected Kuramoto oscillators subject to generic noise.

The model consists of coupled phase-oscillators with different natural frequencies. In the limit of weak coupling, the phases can be modeled using the Kuramoto-type equations

$$\begin{aligned}\frac{d\theta_1}{dt} &= \omega_1 + \frac{K}{2} \sin(\theta_2 - \theta_1) + \eta_1 \\ \frac{d\theta_2}{dt} &= \omega_2 + \frac{K}{2} \sin(\theta_1 - \theta_2) + \eta_2,\end{aligned}\quad (1)$$

where  $\theta_i(t)$  are the oscillator phases,  $\omega_i$  the natural frequencies,  $K$  is the coupling constant, and  $\eta_i$  are stochastic white noise terms satisfying  $\langle \eta_i \rangle = 0$  and  $\langle \eta_i(t) \eta_j(t') \rangle = C_{ij} \delta(t - t')$  with the symmetric and positive semi-definite covariance matrix  $C_{ij} = C_{ji}$ . The model described by Eq. (1) was recently shown to exhibit counter-intuitive enhanced synchronization under uncorrelated noise  $C_{ij} \sim \delta_{ij}$  as opposed to common noise  $C_{ij} = C$  [36]. We now study this effect allowing for arbitrary correlations between the noise terms. It is useful to change variables to the mean angle  $\mu = (\theta_1 + \theta_2)/2$  and angular difference  $\delta = \theta_1 - \theta_2$ . The mean  $\mu$  is irrelevant for synchronization as quantified by the squared Kuramoto order parameter  $R^2 = |\sum_j e^{i\theta_j}/N|^2 = 1/2 + (1/2) \cos \delta$ . We focus on the equation for the phase difference,

$$\delta'(\tau) = 1 - \kappa \sin \delta(\tau) + \zeta, \quad (2)$$

where the prime indicates a derivative with respect to  $\tau = \Delta\omega t$ , the dimensionless parameter  $\kappa = K/\Delta\omega$ , and the dimensionless noise  $\zeta = (\eta_1 - \eta_2)/\Delta\omega$ .

In the absence of noise,  $\zeta = 0$ , it is well known that Eq. (2) exhibits a synchronization transition at  $\kappa = 1$  [44, 47]. To study non-vanishing noise, we calculate  $\langle \zeta \rangle = 0$

\* [henrik.ronellenfitsch@gmail.com](mailto:henrik.ronellenfitsch@gmail.com)

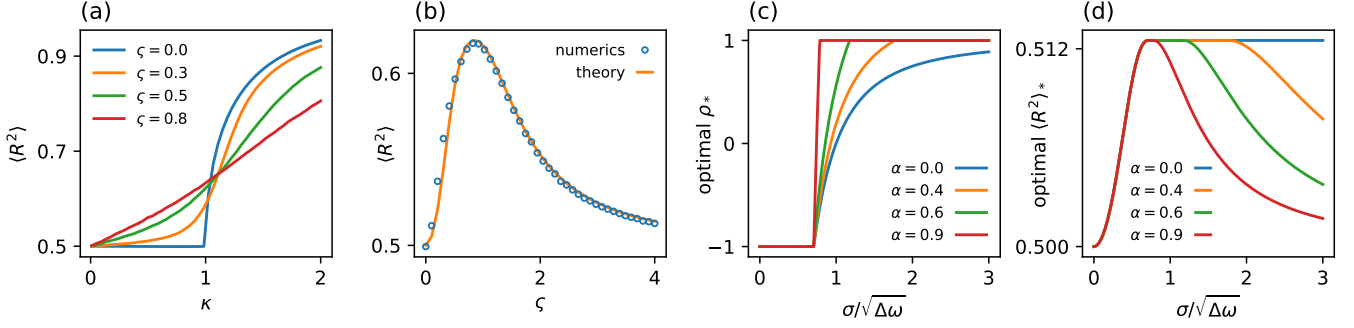


FIG. 1. Noise-enhanced synchronization in the two-oscillator model and optimal covariance transition. (a) Numerically obtained  $\langle R^2 \rangle$  from integrating Eq. (2) until  $\tau = 400000$  from random initial conditions as a function of  $\kappa = K/\Delta\omega$  for several  $\zeta$ . (b) Numerically obtained  $\langle R^2 \rangle$  from integrating Eq. (2) until  $\tau = 20000$  from random initial conditions (circles) and analytic approximation (see Ref. [46], Section I for the explicit formula) as a function of  $\zeta$  for  $\kappa = 0.9$ . (c) Numerically approximated optimal covariance  $\rho_*$ . To simplify comparing between different combinations of  $\sigma_{1,2}$ , we introduced the average  $\sigma = (\sigma_1 + \sigma_2)/2$  and the relative difference  $\alpha = |\sigma_1 - \sigma_2|/(\sigma_1 + \sigma_2)$ . Optimal correlations were obtained at  $\kappa = 0.1$ . The transitions occur at  $\sigma_a/\sqrt{\Delta\omega} \approx 1/\sqrt{2}$  and  $\sigma_c/\sqrt{\Delta\omega} \approx 1/(\alpha\sqrt{2})$ . (d) Approximate optimal order parameter  $\langle R^2 \rangle_*$  for the optimal covariances shown in panel (c) at  $\kappa = 0.1$ .

and

$$\begin{aligned} \langle \zeta(\tau)\zeta(\tau') \rangle &= \frac{1}{\Delta\omega}(C_{11} - 2C_{12} + C_{22})\delta(\tau - \tau') \\ &= 2\zeta^2\delta(\tau - \tau'). \end{aligned}$$

This suggests that  $\zeta^2 = (C_{11} - 2C_{12} + C_{22})/(2\Delta\omega)$  is the relevant effective noise strength for synchronization. This effective noise strength depends on the correlation between the original noise inputs  $\eta_{1,2}$ . Specifically, for common noise,  $C_{ij} = \sigma^2$  implies  $\zeta^2 = 0$ : Common noise does not affect synchronization at all. For uncorrelated noise,  $C_{ii} = \sigma^2$  and  $C_{12} = 0$ , which implies  $\zeta^2 = \sigma^2/\Delta\omega$ . A similar argument shows that the maximum effective noise strength for synchronization is achieved for *anti-correlated* inputs  $C_{ii} = \sigma^2$ ,  $C_{12} = -\sigma^2$  with  $\zeta^2 = 2\sigma^2/\Delta\omega$ .

But how does  $\zeta^2$  affect synchronization, and can we find an optimal noise correlation? We numerically simulated Eq. (2) and computed long-time averages of the order parameter  $\langle R^2 \rangle$  for several  $\zeta^2$ . In the regime below the transition,  $\kappa < 1$ , noise generally enhances synchronization, while for  $\kappa > 1$ , noise generally decreases synchronization [Fig. 1 (a), Ref. [36]]. At fixed  $\kappa$ , there exists an optimal effective noise  $\zeta_*^2$  that maximizes synchronization [Fig. 1 (b)].

We can relate this to the original noise covariance matrix as follows. Fixing the noise variances  $C_{ii} = \sigma_i^2$ , the covariance  $C_{12} = \sigma_1\sigma_2\rho$  with the correlation  $-1 \leq \rho \leq 1$  can be used to tune the effective noise and thus increase synchronization. While it appears straightforward to obtain the optimal  $\zeta_*^2$  and then to solve  $\zeta_*^2 = (\sigma_1^2 - 2\sigma_1\sigma_2\rho + \sigma_2^2)/(2\Delta\omega)$  for the correlation  $\rho$ , the constraint  $-1 \leq \rho \leq 1$  must be taken into account: it is not always possible to adjust  $\rho$  and reach the optimal  $\zeta_*^2$ . When this happens, the optimal correlation occurs at the boundary of the allowed range,  $\rho_* = \pm 1$ . Solving

for  $\rho_*$ , the optimal correlation to enhance synchronization at fixed  $\sigma_{1,2}$  is then

$$\rho_* = \left[ \frac{\sigma_1^2 + \sigma_2^2}{2\sigma_1\sigma_2} - \frac{\zeta_*^2\Delta\omega}{\sigma_1\sigma_2} \right]', \quad (3)$$

where the primed angle brackets indicate that the argument is clipped to remain between  $-1$  and  $1$  using  $[x]' = \min(\max(x, -1), 1)$ . This clipping leads to a sharp transition [Fig. 1 (c,d)]. In the following, it is useful to introduce the average  $\sigma = (\sigma_1 + \sigma_2)/2$ . For small  $\sigma/\sqrt{\Delta\omega}$ , anti-correlated noise optimally enhances synchronization [Fig. 1 (c)]. Solving Eq. (3) for  $\rho_* = -1$ , we find the critical noise strength  $\sigma_a$  below which anti-correlated noise is optimal,  $\sigma_a = \zeta_*\sqrt{\Delta\omega}/2$ . Similarly, solving Eq. (3) for  $\rho_* = +1$ , we find the critical noise strength  $\sigma_c$  above which common noise is optimal,  $\sigma_c = \sigma_a/\alpha$ , where  $\alpha = |\sigma_1 - \sigma_2|/(\sigma_1 + \sigma_2)$ . In the regime where  $-1 < \rho_* < 1$ , the global optimum can be reached and  $\langle R^2 \rangle_*$  is constant. Otherwise, the optimal order parameter occurs at the boundary of the allowed range of  $\rho$  and is less than the global maximum. In this case,  $\rho_* = \pm 1$  [Fig. 1 (c)].

While  $\zeta_*^2$  and thus  $\rho_*$  can be obtained numerically, it is possible to gain insight from an analytic approximation. Equation (2) is equivalent to the Fokker-Planck equation

$$\frac{\partial p(\delta, t)}{\partial t} = -\frac{\partial}{\partial \delta} [(1 - \kappa \sin \delta)p(\delta, t)] + \zeta^2 \frac{\partial^2 p(\delta, t)}{\partial \delta^2} \quad (4)$$

for the probability density  $p(\delta + 2\pi, t) = p(\delta, t)$ . From a Fourier series approximation to the solution of Eq. (4), we obtain an explicit expression for  $\langle R^2 \rangle(\zeta, \kappa)$  in the regime of small  $\kappa$  [46]. The optimal effective noise is then  $\zeta_*^2 = 1 - \frac{23}{100}\kappa^2 + \mathcal{O}(\kappa^4)$ , and the corresponding maximal order parameter is  $\langle R^2 \rangle_* = \frac{1}{2} + \frac{\kappa}{8} + \mathcal{O}(\kappa^3)$ . Even for larger  $\kappa \lesssim 1$ , there is good agreement with full numerical solutions of the Fokker-Planck equation [Fig. 1

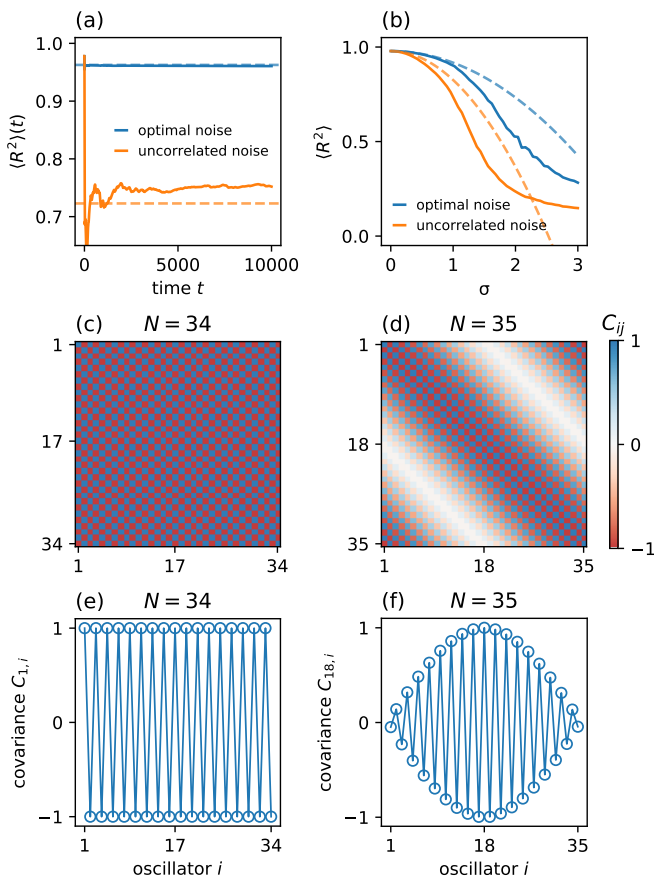


FIG. 2. Optimal noise patterns in periodic oscillator chains near fixed points. (a) Time-averaged order parameter  $\langle R^2 \rangle(t) = (1/t) \int_0^t R^2(t') dt'$  in a periodic chain of  $N = 54$  oscillators for optimal and uncorrelated noise. Dashed lines correspond to model predictions from Eq. (7). The noise variance  $\sigma = 0.5$ . (b) Numerically obtained long-time order parameters  $\langle R^2 \rangle$  in a  $N = 20$  periodic chain of oscillators with optimal and uncorrelated noise. Dashed lines correspond to model predictions, order parameters were obtained at  $t = 15000$ . (c) Optimal covariance matrix for even periodic chain of  $N = 34$ . (d) Optimal covariance matrix for odd periodic chain of  $N = 35$ . (e) Optimal covariances  $C_{1,i}$  with respect to the first oscillator in the even chain. (f) Frustrated optimal covariance pattern  $C_{18,i}$  with respect to the center oscillator in the odd chain. Natural frequencies in all panels were drawn from the Normal distribution  $\mathcal{N}(0, 1/N^2)$ , and  $K = 2$ .

(b), Ref. [46], Section I}. The situation is different in the regime  $\kappa > 1$  where phase-locked fixed points exist. Here, common noise is always optimal and the noise-free order parameter  $R_0^2$  can not be exceeded {Ref. [46], Section II}.

In many real-world cases such as power grids, the network operates near a phase-locked fixed point instead of in the incoherent regime. Therefore, we now focus on general networks near a fixed point and show that, unlike in the two-oscillator case, there exist optimal correlation patterns beyond common noise that enhance synchro-

nization. While we note that other order parameters can also be relevant [48], here consider the Kuramoto order parameter. The equations of motion for  $N$  coupled oscillators are

$$\frac{d\theta_i}{dt} = \omega_i + \sum_{j=1}^N K_{ij} \sin(\theta_j - \theta_i) + \eta_i, \quad (5)$$

where again the stochastic forcing is given by correlated white noise,  $\langle \eta_i(t) \eta_j(t') \rangle = C_{ij} \delta(t - t')$  and  $\langle \eta_i \rangle = 0$ . The matrix  $K_{ij} = K_{ji}$  encodes the weighted network topology. Equation (5) as well as the order parameter allow to shift the phases as  $\theta_i \rightarrow \theta_i - \mu$ , where  $\mu$  is the mean phase. In the following, we adopt these ‘‘centered dynamics,’’ where the mean natural frequency, the mean noise, and the mean covariance with any oscillator vanish,  $\sum_i \omega_i = \sum_j \eta_j = \sum_j C_{ij} = 0$  {Ref. [46], Section III}. Note that noise that is uncorrelated in the original frame ( $C_{ij} \sim \delta_{ij}$ ) appears uniformly correlated in centered dynamics,  $C_{ij} \sim \delta_{ij} + (\delta_{ij} - 1)/(N - 1)$ . Assuming that weak noise drives the centered Eq. (5) near a fixed point  $0 = \omega_i + \sum_{j=1}^N K_{ij} \sin(\bar{\theta}_j - \bar{\theta}_i)$ , we expand  $\theta_i = \bar{\theta}_i + \varepsilon_i$  to obtain the linearized dynamics of the perturbations  $\varepsilon_i$ ,

$$\frac{d\varepsilon_i}{dt} = \sum_{j=1}^N K_{ij} \cos(\bar{\theta}_j - \bar{\theta}_i) (\varepsilon_j - \varepsilon_i) + \eta_i. \quad (6)$$

In the following, we are interested in long-time averages such that any initial transients have decayed and the system has settled into an equilibrium distribution. We expand the order parameter averaged in this way,

$$\langle R^2 \rangle = R_0^2 + \frac{1}{2} \langle \varepsilon^\top H \varepsilon \rangle + \mathcal{O}(\varepsilon^3), \quad (7)$$

where  $R_0^2$  is the order parameter at the fixed point  $\bar{\theta}_i$ , and the angle brackets denote the long-time average. The linear term  $\langle J \varepsilon \rangle = J \langle \varepsilon \rangle$ , where  $J$  is the Jacobian matrix, vanishes due to  $\langle \varepsilon \rangle = 0$ . The Hessian matrix  $H_{ij} = (2/N^2) (\cos(\bar{\theta}_i - \bar{\theta}_j) - \delta_{ij} \sum_k \cos(\bar{\theta}_i - \bar{\theta}_k))$ , encodes the synchronization state of the fixed point and is negative semi-definite close to the synchronous state  $\bar{\theta}_i \approx 0$  {Ref. [46], Section VI}, but can be positive semi-definite or even indefinite, for instance close to ‘‘twisted states’’ {Refs. [49] and [46], Section VI}. Thus, we expect that noise will generically reduce synchrony. However, it is still possible to find noise inputs that minimize these effects, and transitions can occur. Equation (7) suggests that such optimal synchronization is achieved by maximizing the second order term  $\langle \varepsilon^\top H \varepsilon \rangle = \text{tr}(HE)$ . Here,  $\text{tr}(\cdot)$  is the matrix trace, and  $E = \langle \varepsilon \varepsilon^\top \rangle$  satisfies the continuous Lyapunov equation  $LE + EL = -C$  for the weighted Laplacian matrix  $L_{ij} = K_{ij} \cos(\bar{\theta}_j - \bar{\theta}_i) - \delta_{ij} \sum_n K_{in} \cos(\bar{\theta}_n - \bar{\theta}_i)$ . This can be seen by formally solving Eq. (6) in the Langevin formalism and performing the noise average {Ref. [46], Section V}. The Lyapunov equation frequently occurs in stability and control theory [50]. Our goal of finding

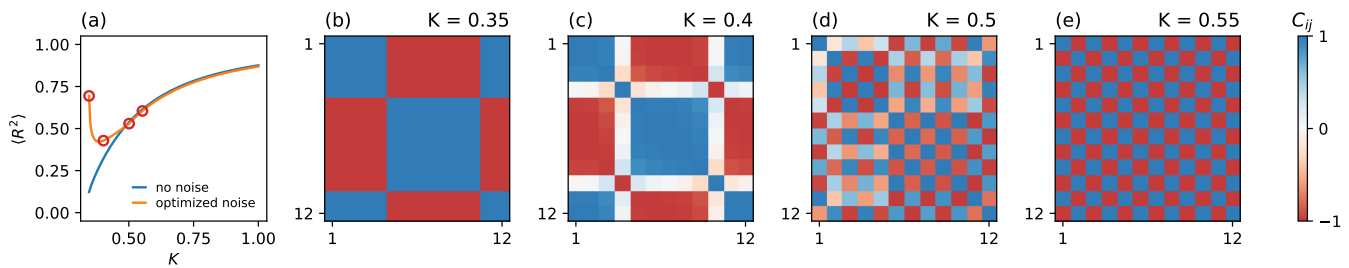


FIG. 3. Optimal noise covariance matrix near the synchronization transition in an  $N = 12$  oscillator chain. (a) Optimal noise significantly enhances the approximate order parameter  $\langle R^2 \rangle = R_0^2 + (1/2)\sigma^2 \text{tr}(HE)$  close to the synchronization transition. Shown are curves with  $\sigma = 0.25$  and  $\sigma = 0$  (no noise). (b–e) Optimal covariance matrices near the synchronization transition. The locations corresponding to the matrices in panels (b–e) are marked (red circles) in panel (a). Close to the phase-drift regime (small  $K$ ), the optimal covariances are large-scale ordered and then transition to local order.

the optimal noise covariances  $C$  can be formulated as the constrained optimization problem

$$\begin{aligned} \max_{C,E} \quad & \text{tr}(HE) \\ \text{such that} \quad & LE + EL = -C \\ & C \succeq 0. \end{aligned} \quad (8)$$

A valid covariance matrix must be positive semi-definite,  $C \succeq 0$ . This constraint turns the problem into a semi-definite program [51]. As it stands, the optimization problem is unbounded, such that we must augment it by an additional constraint to set the noise scale. For simplicity, we fix uniform variances,  $C_{ii} = 1$ . Because the Lyapunov equation in Eq. (8) is linear, any uniform  $C_{ii}$  can be obtained by rescaling the optimal solution. Due to the centered frame constraint  $\sum_j C_{ij} = 0$  we expect anticorrelations to be relevant in complex networks again.

To uncover the relationship between network topology and optimal noise, we numerically analyze networks of increasing complexity. For simplicity, we take the coupling constants to be uniform,  $K_{ij} \equiv K/d$ , where  $d$  is the network’s average degree. We draw the natural frequencies from a Gaussian distribution  $\omega_i \sim \mathcal{N}(0, 1/N^2)$ , where  $N$  is the number of nodes. The mean of the natural frequencies for each network is set to exactly zero. Fixed points and solutions to the semi-definite program Eq. (8) are obtained numerically {Ref. [46], Section IV}.

As the simplest extension of our two-oscillator model we first consider periodic chains of  $N$  oscillators. We note that the optimal noise pattern obtained from solving Eq. (8) is highly effective in improving synchronization as compared to uncorrelated noise [Fig. 2 (a)], even far into the nonlinear regime [Fig. 2 (b)]. Interestingly, the optimal noise is such that neighboring pairs in chains with an even number of oscillators receive anti-correlated inputs [Fig. 2 (c,e)]. However, it is not always possible for all pairs of neighbors in a network to receive perfectly anti-correlated inputs, leading to frustrated patterns of optimal noise. Indeed, for an odd number of oscillators in the chain, the magnitude of the optimal noise corre-

lation  $|C_{ij}|$  decays away from any particular oscillator  $i$ . The chain topology prevents any two neighboring oscillators from receiving perfectly anti-correlated noise [Fig. 2 (d,f)]. This effect is also seen in periodic grids {Ref. [46], Section VIII}. It is interesting to note that the optimal noise itself may exhibit a transition from local to global organization near the synchronization transition of the underlying network, depending on the specific set of natural frequencies  $\omega_i$  (Fig. 3). The transition is accompanied by a significant increase of the order parameter [Fig. 3 (a)] that even persists into the phase-drift regime for a large region of couplings  $K$  {Ref. [46], Section IX}.

We finally consider complex network topologies derived from power grids [52]. Here, the optimal noise patterns show clustering, where groups of oscillators are approximately anti-correlated among themselves. Correlations between the clusters are approximately zero (Fig. 4), potentially promoting cluster synchronization [53]. One particular type of cluster in these networks consists of one single “dangling” node together with its neighbor. Such nodes have been identified as vulnerable to perturbations before [54, 55]. Real power grid dynamics can be modeled using a second-order model [9] which is also amenable to our method and shows a dependence of the optimal covariances on the inertia in the network {Ref. [46], Section X}.

We studied to what extent synchronization in complex oscillator networks can be enhanced by correlated noise. We showed that in the phase-drift regime of a two-oscillator system, optimal noise correlations can significantly improve synchronization. The optimal correlations exhibit a transition between anti-correlated and correlated noise depending on the overall noise strength. In complex networks, we found that the optimal input noise is generally anti-correlated with diverse patterns where the strength of correlations can be constant, decaying, or even be restricted to clusters of oscillators.

Our results may have implications for real networks such as power grids and neuronal networks. For instance, power grid synchronization may be enhanced if new power plants and lines are judiciously placed ac-



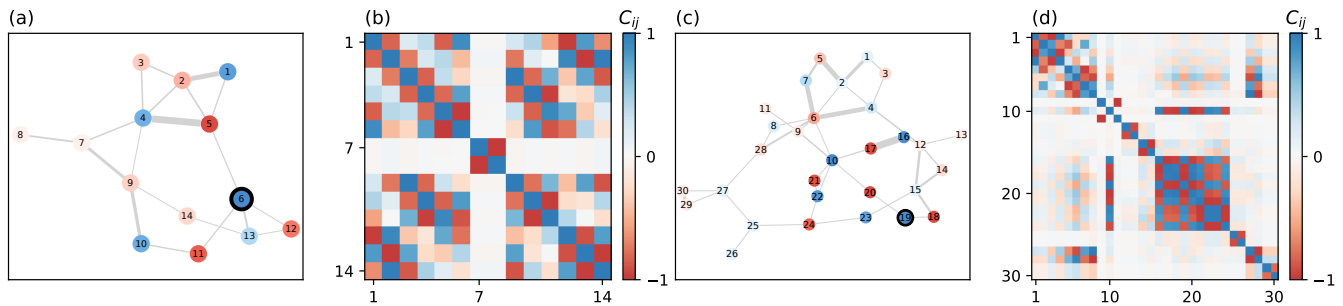


FIG. 4. Anti-correlated patterns form clusters in complex networks. (a) IEEE 14-node test grid, node colors corresponds to correlation with oscillator 6. (b) Optimal covariance matrix for the network from (a). There are two clusters of anti-correlated oscillators that are uncorrelated with each other. (c) IEEE 30-node test grid, node colors corresponds to correlation with oscillator 19. (d) Optimal covariance matrix for the network from (c). There are several clusters of anti-correlated oscillators that are uncorrelated with each other. Small clusters of two nodes generally have one of the nodes “dangling” with only one neighbor. In all graph plots, edge width is proportional to the coupling strength  $K_{ij}$ . Power loads were centered and normalized to unit variance, and then used as constant inputs.

ording to the principles outlined above. Correlations of input noise can be estimated [56], or predicted from the weather [57, 58]. Our work opens up new pathways to understanding and controlling synchronization in complex systems.

## ACKNOWLEDGMENTS

S.M., T.S., and T.T.C. acknowledge support from the Williams College Science Center.

- 
- [1] B. Lindner, Effects of noise in excitable systems, *Physics Reports* **392**, 321 (2004).
- [2] D. K. Wells, W. L. Kath, and A. E. Motter, Control of Stochastic and Induced Switching in Biophysical Networks, *Physical Review X* **5**, 031036 (2015).
- [3] W. Bialek, Physical Limits to Sensation and Perception, *Annual Review of Biophysics and Biophysical Chemistry* **16**, 455 (1987).
- [4] L. S. Tsimring, Noise in biology, *Reports on Progress in Physics* **77**, 026601 (2014).
- [5] J. Shlens, F. Rieke, and E. Chichilnisky, Synchronized firing in the retina, *Current Opinion in Neurobiology* **18**, 396 (2008).
- [6] H. G. Eyherabide and I. Samengo, When and Why Noise Correlations Are Important in Neural Decoding, *Journal of Neuroscience* **33**, 17921 (2013).
- [7] I. Kanitscheider, R. Coen-Cagli, and A. Pouget, Origin of information-limiting noise correlations, *Proceedings of the National Academy of Sciences* **112**, E6973 (2015).
- [8] M. H. Matheny, J. Emenheiser, W. Fon, A. Chapman, A. Salova, M. Rohden, J. Li, M. Hudoba de Badyn, M. Pósfai, L. Duenas-Osorio, M. Mesbahi, J. P. Crutchfield, M. C. Cross, R. M. D’Souza, and M. L. Roukes, Exotic states in a simple network of nanoelectromechanical oscillators, *Science* **363**, eaav7932 (2019).
- [9] P. H. Nardelli, N. Rubido, C. Wang, M. S. Baptista, C. Pomalaza-Raez, P. Cardieri, and M. Latva-aho, Models for the modern power grid, *The European Physical Journal Special Topics* **223**, 2423 (2014).
- [10] P. Milan, M. Wächter, and J. Peinke, Turbulent Character of Wind Energy, *Physical Review Letters* **110**, 138701 (2013).
- [11] B. Schäfer, C. Beck, K. Aihara, D. Witthaut, and M. Timme, Non-Gaussian power grid frequency fluctuations characterized by Lévy-stable laws and superstatistics, *Nature Energy* **3**, 119 (2018).
- [12] S. Strogatz, *Sync: How Order Emerges from Chaos In the Universe, Nature, and Daily Life* (Hachette Books, 2012).
- [13] R. E. Mirollo and S. H. Strogatz, Synchronization of Pulse-Coupled Biological Oscillators, *SIAM Journal on Applied Mathematics* **50**, 1645 (1990).
- [14] C. Luo and H. Banakar, Strategies to smooth wind power fluctuations of wind turbine generator, *IEEE Transactions on Energy Conversion* **22**, 341 (2007).
- [15] B. C. Bag, K. G. Petrosyan, and C.-K. Hu, Influence of noise on the synchronization of the stochastic Kuramoto model, *Physical Review E* **76**, 056210 (2007).
- [16] T. Yanagita and A. S. Mikhailov, Design of oscillator networks with enhanced synchronization tolerance against noise, *Physical Review E* **85**, 056206 (2012).
- [17] H. Ronellenfitsch, J. Dunkel, and M. Wilczek, Optimal Noise-Canceling Networks, *Physical Review Letters* **121**, 208301 (2018).
- [18] J. Hindes, P. Jacquod, and I. B. Schwartz, Network desynchronization by non-Gaussian fluctuations, *Physical Review E* **100**, 052314 (2019).
- [19] M. Tyloo, T. Coletta, and P. Jacquod, Robustness of Synchrony in Complex Networks and Generalized Kirchhoff Indices, *Physical Review Letters* **120**, 084101 (2018).
- [20] M. Fazlyab, F. Dörfler, and V. M. Preciado, Optimal network design for synchronization of coupled oscillators, *Automatica* **84**, 181 (2017).
- [21] T. Tanaka and T. Aoyagi, Optimal weighted networks of

- phase oscillators for synchronization, *Physical Review E* **78**, 046210 (2008).
- [22] M. Brede, Synchrony-optimized networks of non-identical Kuramoto oscillators, *Physics Letters A* **372**, 2618 (2008).
- [23] B. Li and K. Y. M. Wong, Optimizing synchronization stability of the Kuramoto model in complex networks and power grids, *Physical Review E* **95**, 012207 (2017).
- [24] D. Kelly and G. A. Gottwald, On the topology of synchrony optimized networks of a Kuramoto-model with non-identical oscillators, *Chaos: An Interdisciplinary Journal of Nonlinear Science* **21**, 025110 (2011).
- [25] M. Fardad, F. Lin, and M. R. Jovanovic, Design of Optimal Sparse Interconnection Graphs for Synchronization of Oscillator Networks, *IEEE Transactions on Automatic Control* **59**, 2457 (2014).
- [26] P. S. Skardal, D. Taylor, and J. Sun, Optimal synchronization of complex networks, *Physical Review Letters* **113**, 1 (2014).
- [27] F. Dörfler and F. Bullo, Synchronization and Transient Stability in Power Networks and Nonuniform Kuramoto Oscillators, *SIAM Journal on Control and Optimization* **50**, 1616 (2012).
- [28] M. Alhazmi, P. Dehghanian, S. Wang, and B. Shinde, Power Grid Optimal Topology Control Considering Correlations of System Uncertainties, *IEEE Transactions on Industry Applications* **55**, 5594 (2019).
- [29] M. Durand, Structure of Optimal Transport Networks Subject to a Global Constraint, *Physical Review Letters* **98**, 088701 (2007).
- [30] S. Bohn and M. O. Magnasco, Structure, Scaling, and Phase Transition in the Optimal Transport Network, *Physical Review Letters* **98**, 088702 (2007).
- [31] E. Katifori, G. J. Szöllösi, and M. O. Magnasco, Damage and Fluctuations Induce Loops in Optimal Transport Networks, *Physical Review Letters* **104**, 048704 (2010).
- [32] J. W. Rocks, H. Ronellenfitsch, A. J. Liu, S. R. Nagel, and E. Katifori, Limits of multifunctionality in tunable networks, *Proceedings of the National Academy of Sciences* **116**, 2506 (2019).
- [33] J. B. Kirkegaard and K. Sneppen, Optimal Transport Flows for Distributed Production Networks, *Physical Review Letters* **124**, 208101 (2020).
- [34] F. Kaiser, H. Ronellenfitsch, and D. Witthaut, Discontinuous transition to loop formation in optimal supply networks, *Nature Communications* **11**, 5796 (2020).
- [35] H. Ronellenfitsch, Optimal Elasticity of Biological Networks, *Physical Review Letters* **126**, 038101 (2021).
- [36] Z. G. Nicolaou, M. Sebek, I. Z. Kiss, and A. E. Motter, Coherent Dynamics Enhanced by Uncorrelated Noise, *Physical Review Letters* **125**, 094101 (2020).
- [37] J. H. Meng and H. Riecke, Synchronization by uncorrelated noise: interacting rhythms in interconnected oscillator networks, *Scientific Reports* **8**, 6949 (2018).
- [38] K. H. Nagai and H. Kori, Noise-induced synchronization of a large population of globally coupled nonidentical oscillators, *Physical Review E* **81**, 065202 (2010).
- [39] H. Nakao, K. Arai, and Y. Kawamura, Noise-Induced Synchronization and Clustering in Ensembles of Uncoupled Limit-Cycle Oscillators, *Physical Review Letters* **98**, 184101 (2007).
- [40] C. Zhou, J. Kurths, I. Z. Kiss, and J. L. Hudson, Noise-Enhanced Phase Synchronization of Chaotic Oscillators, *Physical Review Letters* **89**, 014101 (2002).
- [41] H. Nakao, Phase reduction approach to synchronisation of nonlinear oscillators, *Contemporary Physics* **57**, 188 (2016).
- [42] M. Aravind, S. Sinha, and P. Parmananda, Competitive interplay of repulsive coupling and cross-correlated noises in bistable systems, *Chaos: An Interdisciplinary Journal of Nonlinear Science* **31**, 061106 (2021).
- [43] R. K. Esfahani, F. Shahbazi, and K. A. Samani, Noise-induced synchronization in small world networks of phase oscillators, *Physical Review E* **86**, 036204 (2012).
- [44] Y. Kuramoto, *Chemical Oscillations, Waves, and Turbulence*, Springer Series in Synergetics, Vol. 19 (Springer, Berlin, Heidelberg, 1984).
- [45] J. A. Acebrón, L. L. Bonilla, C. J. Pérez Vicente, F. Ritort, and R. Spigler, The Kuramoto model: A simple paradigm for synchronization phenomena, *Reviews of Modern Physics* **77**, 137 (2005).
- [46] See Supplemental Material below for the explicit analytical expression for the two-oscillator order parameter, an analysis of the approximations made in the main text, derivations of the two-oscillator model near a fixed point, centered dynamics, a derivation of the Lyapunov equation constraint, explanation of numerical methods, optimal noise for twisted states and periodic square grids, an analysis of the parametric dependence of the optimal noise matrices, and an analysis of second-order power grid models. The Supplemental Material includes Refs. [9, 49, 50, 59–61].
- [47] F. Dörfler and F. Bullo, On the Critical Coupling for Kuramoto Oscillators, *SIAM Journal on Applied Dynamical Systems* **10**, 1070 (2011).
- [48] M. Schröder, M. Timme, and D. Witthaut, A universal order parameter for synchrony in networks of limit cycle oscillators, *Chaos: An Interdisciplinary Journal of Nonlinear Science* **27**, 073119 (2017).
- [49] D. A. Wiley, S. H. Strogatz, and M. Girvan, The size of the sync basin, *Chaos: An Interdisciplinary Journal of Nonlinear Science* **16**, 015103 (2006).
- [50] Z. Gajić and M. T. J. Qureshi, *Lyapunov Matrix Equation in System Stability and Control* (Dover Publications, Mineola, NY, 2008) p. 272.
- [51] L. Vandenberghe and S. Boyd, Semidefinite Programming, *SIAM Review* **38**, 49 (1996).
- [52] University of Washington, [Power systems test case archive](#).
- [53] G. V. Osipov, J. Kurths, and C. Zhou, *Synchronization in Oscillatory Networks* (Springer-Verlag, Berlin Heidelberg, 2007) p. 373.
- [54] M. Tyloo, L. Pagnier, and P. Jacquod, The key player problem in complex oscillator networks and electric power grids: Resistance centralities identify local vulnerabilities, *Science Advances* **5**, eaaw8359 (2019).
- [55] D. Manik, M. Rohden, H. Ronellenfitsch, X. Zhang, S. Hallerberg, D. Witthaut, and M. Timme, Network susceptibilities: Theory and applications, *Physical Review E* **95**, 012319 (2017).
- [56] L. Zhu and J. Lin, Learning Spatiotemporal Correlations for Missing Noisy PMU Data Correction in Smart Grid, *IEEE Internet of Things Journal* **8**, 7589 (2021).
- [57] P. E. Bett and H. E. Thornton, The climatological relationships between wind and solar energy supply in Britain, *Renewable Energy* **87**, 96 (2016).
- [58] K. van der Wiel, H. C. Bloomfield, R. W. Lee, L. P. Stoop, R. Blackport, J. A. Screen, and F. M. Selden, The

- influence of weather regimes on European renewable energy production and demand, *Environmental Research Letters* **14**, 094010 (2019).
- [59] C. Rackauckas and Q. Nie, DifferentialEquations.jl—a performant and feature-rich ecosystem for solving differential equations in Julia, *Journal of Open Research Software* **5** (2017).
- [60] M. Udell, K. Mohan, D. Zeng, J. Hong, S. Diamond, and S. Boyd, Convex optimization in Julia, in *2014 First Workshop for High Performance Technical Computing in Dynamic Languages* (2014) pp. 18–28.
- [61] M. Garstka, M. Cannon, and P. Goulart, COSMO: A Conic Operator Splitting Method for Convex Conic Problems, *Journal of Optimization Theory and Applications* **190**, 779 (2021).

## SUPPLEMENTAL MATERIAL

### I. APPROXIMATE SOLUTION OF THE FOKKER-PLANCK EQUATION

While Eq. (4) can not be solved analytically, in the regime of  $\kappa \ll 1$ , the steady-state distribution appears to be well-represented by sinusoids. Encouraged by this, we approximate the steady-state distribution as a truncated Fourier series,  $p(\delta) \approx \sum_{k=-N}^N a_k e^{ik\delta}$ . The normalization condition  $\int_{-\pi}^{\pi} p(\delta) d\delta = 1$  implies  $a_0 = 1/(2\pi)$  and reality of the solution is equivalent to  $a_{-k} = a_k^*$ . Plugging in the shortest non-trivial Fourier series with  $N = 2$  and solving the resulting system of equations yields the following approximation for the Fourier coefficients,

$$\begin{aligned} a_0 &= \frac{1}{2\pi} \\ a_1 &= \frac{1}{2\pi} \frac{2\kappa (2\zeta^2 + i)}{\kappa^2 + 8\zeta^4 + 12i\zeta^2 - 4} \\ a_2 &= \frac{1}{2\pi} \frac{\kappa^2}{\kappa^2 + 8\zeta^4 + 12i\zeta^2 - 4}. \end{aligned}$$

Using this Fourier approximation, we can calculate the expected order parameter as

$$\begin{aligned} \langle R^2 \rangle &= \frac{1}{2} + \frac{1}{2} \langle \cos \delta \rangle = \frac{1}{2} + \frac{\pi}{2} (a_1 + a_1^*) \\ &= \frac{1}{2} + \frac{2\kappa\zeta^2 (\kappa^2 + 8\zeta^4 + 2)}{(\kappa^2 - 4)^2 + 16(\kappa^2 + 5)\zeta^4 + 64\zeta^8} \end{aligned} \quad (\text{S1})$$

where the expectation value is defined as  $\langle f(\delta) \rangle = \int_{-\pi}^{\pi} f(\delta) p(\delta) d\delta$ . This equation can be optimized directly with respect to  $\zeta$  by setting the derivative to zero and solving in Mathematica.

The first approximation found above can be compared to numerical solutions. Specifically, we are interested in the optimal effective noise strength  $\zeta_*^2$  and the corresponding optimal order parameter  $\langle R^2 \rangle_*$ . We solved the Fokker-Planck equation Eq. (4) numerically using Mathematica and numerically obtained  $\zeta_*^2$  and  $\langle R^2 \rangle_*$  using a Golden Section search (termination accuracy was set to  $10^{-6}$ ) as a function of  $\kappa$ . Except for values of  $\kappa$  close to 1, the approximation formulas are very good (Fig. S1).

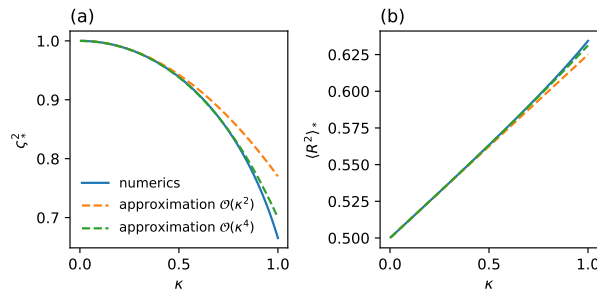


FIG. S1. Comparison of the approximation formulas derived in the main text to corresponding numerically obtained optimal values from a full numerical solution of the Fokker-Planck equation Eq. (4). (a) Optimal effective noise strength where the approximation formula is  $\zeta_*^2 \approx 1 - 23\kappa^2/100 - 1757\kappa^4/25000$ . Note that in the main paper, only the expression to order  $\mathcal{O}(\kappa^2)$  is given. (b) Optimal order parameter where the approximation formula is  $\langle R^2 \rangle_* \approx 1/2 + \kappa/8 + \kappa^3/160$ . Note that in the main paper, only the expression to order  $\mathcal{O}(\kappa)$  is given. The colored lines have the same interpretation as in panel (a).

### II. TWO-OSCILLATOR MODEL NEAR A FIXED POINT

Here, we analyze the two-oscillator model near a fixed point. We start by computing the fixed point in the noise-free case,

$$\delta' = 0 \Rightarrow \bar{\delta} = \arcsin(\kappa^{-1}).$$



We now expand the equation of motion with noise close to the fixed point,  $\delta(\tau) = \bar{\delta} + \varepsilon(\tau)$  as

$$\begin{aligned}\delta' &= \varepsilon' = 1 - \kappa \sin(\bar{\delta} + \varepsilon) + \zeta \\ &\approx -\sqrt{1 - \kappa^{-2}} \varepsilon + \zeta.\end{aligned}\tag{S2}$$

We can similarly expand the order parameter,

$$\begin{aligned}R^2 &= \frac{1}{2} + \frac{1}{2} \cos(\bar{\delta} + \varepsilon) \\ &= R_0^2 - \frac{1}{2\kappa} \varepsilon - \frac{1}{4} \sqrt{1 - \kappa^{-2}} \varepsilon^2 + \mathcal{O}(\varepsilon^3),\end{aligned}\tag{S3}$$

where  $R_0^2 = (1/2)(1 + \sqrt{1 - \kappa^{-2}})$ . Averaging Eq. (S3) over the noise, the term linear in  $\varepsilon$  drops out and we are left with

$$\langle R^2 \rangle = R_0^2 - \frac{1}{4} \sqrt{1 - \kappa^{-2}} \langle \varepsilon^2 \rangle.$$

To calculate the average  $\langle \varepsilon^2 \rangle$ , we formally solve Eq. (S2) as

$$\varepsilon(\tau) = \varepsilon_0 e^{-\sqrt{1 - \kappa^{-2}} \tau} + e^{-\sqrt{1 - \kappa^{-2}} \tau} \int_0^\tau ds e^{\sqrt{1 - \kappa^{-2}} s} \zeta(s).$$

For long times, the first term vanishes and we can use the second term to calculate

$$\begin{aligned}\langle \varepsilon(\tau)^2 \rangle &= e^{-2\sqrt{1 - \kappa^{-2}} \tau} \int_0^\tau ds \int_0^\tau ds' \langle \zeta(s) \zeta(s') \rangle e^{\sqrt{1 - \kappa^{-2}}(s+s')} \\ &= \int_0^\tau dy \int_0^\tau dy' \langle \zeta(\tau - y) \zeta(\tau - y') \rangle e^{-\sqrt{1 - \kappa^{-2}}(y+y')}, \\ &= 2\zeta^2 \int_0^\tau dy \int_0^\tau dy' \delta(y' - y) e^{-\sqrt{1 - \kappa^{-2}}(y+y')},\end{aligned}$$

where we substituted  $y = \tau - s$ ,  $y' = \tau - s'$ . Taking the limit  $\tau \rightarrow \infty$ , we end up with

$$\langle \varepsilon^2 \rangle = 2\zeta^2 \int_0^\infty dy e^{-2\sqrt{1 - \kappa^{-2}} y} = \frac{\zeta^2}{\sqrt{1 - \kappa^{-2}}}.$$

Plugging this expression back into Eq. (S3), we obtain

$$\langle R^2 \rangle = R_0^2 - \frac{1}{4} \zeta^2.$$

### III. CENTERED DYNAMICS OF COMPLEX NETWORKS

Eq. (5) from the main paper contains a freedom of re-defining  $\theta_i \rightarrow \theta_i + c$  for some constant  $c$  corresponding to a reference angle. Here, we fix this freedom by introducing the new variables

$$\begin{aligned}\delta_i(t) &= \theta_i(t) - \mu(t) \\ \mu(t) &= \frac{1}{N} \sum_j \theta_j(t).\end{aligned}$$

Taking derivatives and plugging them into Eq. (1), we find that they satisfy

$$\dot{\delta}_i = \omega_i - \frac{1}{N} \sum_j \omega_j(t) + \sum_j K_{ij} \sin(\delta_i - \delta_j) + \eta_i - \frac{1}{N} \sum_j \eta_j(t)\tag{S4}$$

$$\dot{\mu} = \frac{1}{N} \sum_j \omega_j(t) + \frac{1}{N} \sum_j \eta_j(t),\tag{S5}$$

where we used  $\sum_{i,j} K_{ij} \sin(\delta_i - \delta_j) = 0$  due to antisymmetry. Equation (S4) is equivalent to Eq. (5) but with centered inputs,  $\omega_i \rightarrow \omega_i - (1/N) \sum_j \omega_j(t)$  and  $\eta_i \rightarrow \eta_i - (1/N) \sum_j \eta_j(t)$ . The order parameter  $R^2$  is independent of  $\mu$ , so it is sufficient to consider centered dynamics and assume that  $\sum_j \omega_j = 0$ . However, we must consider the effect of centering on the stochastic inputs. Specifically, the centered noisy inputs can be written using a projection matrix  $Q$  as

$$Q\boldsymbol{\eta} = \left( \mathbb{1} - \frac{1}{N} J \right) \boldsymbol{\eta},$$

where  $J_{ij} = 1$ . Similarly, if  $\langle \eta_i(t) \eta_j(t') \rangle = C_{ij} \delta(t - t')$ , then the centered correlation matrix is

$$Q \langle \boldsymbol{\eta}(t) \boldsymbol{\eta}^\top(t') \rangle Q^\top = Q C Q \delta(t - t'). \quad (\text{S6})$$

Thus, the centered covariances are constrained to have vanishing row and column sums,  $\sum_j C_{ij} = \sum_i C_{ij} = 0$ . This is also automatically enforced by the Lyapunov equation constraint in Eq. (8).

## IV. NUMERICAL METHODS

### A. Numerical method for obtaining fixed points

Fixed points  $\bar{\theta}_i$  satisfy

$$0 = \omega_i + \sum_j K_{ij} \sin(\bar{\theta}_j - \bar{\theta}_i)$$

and are found using a Trust-Region method as implemented in the `NLSolve.jl` package for the Julia language. As initial guess we use random numbers drawn from a normal distribution with mean 0 and standard deviation 0.01.

### B. Numerical integration of the dynamical equations

The dynamics in the main paper can be brought into the form of a system of stochastic differential equations,

$$d\mathbf{X} = \mathbf{f}(\mathbf{X}, t) dt + G d\mathbf{W}.$$

Here,  $\mathbf{f}(\mathbf{X}, t)$  is the deterministic dynamics and  $d\mathbf{W}$  is a vector of white noise terms. Finally,  $G$  is a matrix describing the correlations between the individual noise terms. For instance,  $G = \mathbb{1}$  corresponds to uncorrelated white noise. In our work, we prescribe the correlation matrix  $C$  between the noise terms,

$$C = \langle G d\mathbf{W} d\mathbf{W}^\top G^\top \rangle = G \underbrace{\langle d\mathbf{W} d\mathbf{W}^\top \rangle}_{=\mathbb{1}} G^\top = G G^\top, \quad (\text{S7})$$

where we used the fact that  $d\mathbf{W}$  is uncorrelated white noise. To construct a matrix  $G$  satisfying Eq. (S7), we use the singular value decomposition of  $C$ ,

$$C = U \Sigma U^\top = U \sqrt{\Sigma} U^\top U \sqrt{\Sigma} U^\top.$$

Here, we used that  $C$  is symmetric and added in a factor of  $U^\top U = \mathbb{1}$  to end up with a symmetric  $G = U \sqrt{\Sigma} U^\top$  (this specific choice has no bearing on the results).

To efficiently calculate the long-time averaged order parameter without the need to store the entire time series, we note that any time average  $y(t) = \langle f(t) \rangle = \frac{1}{t} \int_0^t f(t') dt'$  satisfies the differential equation

$$y'(t) = \frac{f(t) - y(t)}{t}, \quad (\text{S8})$$

with the initial condition  $y(0) = f(0)$  and  $y'(0) = \frac{1}{2} f'(0)$ . Equation (S8) with  $f(t) = R^2(t)$  is solved concurrently with the original SDE and produces the averaged order parameter.

The complete system of SDEs is numerically solved using the `DifferentialEquations.jl` package [59] in the Julia language with an Euler-Maruyama scheme and time-step  $\Delta t = 0.01$ .

### C. Numerical optimization

Numerical optimization of the problem given by Eq. (8) is done by implementing it in the domain-specific language of the `Convex.jl` package [60] for the Julia language. The problem is then solved using the COSMO algorithm [61] with convergence tolerances  $\varepsilon_{\text{rel}} = \varepsilon_{\text{abs}} = 10^{-7}$ .

## V. DERIVATION OF THE LYAPUNOV EQUATION CONSTRAINT

Here, we compute the variance of fluctuations directly in the Langevin formalism. We are interested in the long-term limit where any initial transients have decayed, and the system has relaxed to a stationary distribution.

We consider the linearized first-order system from the main paper,

$$\dot{\boldsymbol{\varepsilon}} = L\boldsymbol{\varepsilon} + \boldsymbol{\eta}(t),$$

where  $\langle \boldsymbol{\eta} \rangle = \mathbf{0}$ ,  $\langle \boldsymbol{\eta}(t)\boldsymbol{\eta}(t')^\top \rangle = C\delta(t-t')$  is white noise input in time with centered correlation matrix  $C$  and  $L$  is the weighted graph Laplacian with components  $L_{ij} = K_{ij} \cos(\bar{\theta}_j - \bar{\theta}_i) - \delta_{ij} \sum_n K_{in} \cos(\bar{\theta}_n - \bar{\theta}_i)$ . The solution to this system can be expressed as

$$\boldsymbol{\varepsilon}(t) = \exp(Lt)\boldsymbol{\varepsilon}_0 + \int_0^t \exp(L(t-s))\boldsymbol{\eta}(s) ds.$$

As long as the network graph is connected, the Laplacian has a single vector in its nullspace, the vector of all 1s  $\mathbf{1} = (1, 1, \dots, 1)^\top$ , and is otherwise negative definite. The centered dynamics introduced in the previous section are equivalent to  $\mathbf{1}^\top \boldsymbol{\varepsilon}$ , such that all solutions to the linear differential equation live in the space orthogonal to the Laplacian's nullspace. Thus, the homogeneous solution  $\exp(Lt)\boldsymbol{\varepsilon}_0 = \sum_{j=2}^N e^{\lambda_j t} (\mathbf{u}_j^\top \boldsymbol{\varepsilon}_0) \mathbf{u}_j$ , where  $\lambda_j < 0$  are the nonzero eigenvalues and  $\mathbf{u}_j$  the corresponding eigenvectors of  $L$ , decays for large times, and we can focus on the particular solution.

We want to compute the matrix of equal-time covariances in the long-time limit,

$$\begin{aligned} \langle \boldsymbol{\varepsilon}(t)\boldsymbol{\varepsilon}(t)^\top \rangle &= \int_0^t ds \int_0^t ds' \exp(L(t-s)) \langle \boldsymbol{\eta}(s)\boldsymbol{\eta}(s')^\top \rangle \exp(L(t-s')) \\ &= \int_0^t ds \int_0^t ds' \exp(L(t-s)) C \exp(L(t-s')) \delta(s-s') \\ &= \int_0^t dy \int_0^t dy' \exp(Ly) C \exp(Ly') \delta(y'-y). \end{aligned} \quad (\text{S9})$$

We substituted  $y = t - s$ ,  $y' = t - s'$ , and used the fact that  $\langle \boldsymbol{\eta}(t)\boldsymbol{\eta}^\top(t') \rangle = C\delta(t-t')$ . We now take the limit  $t \rightarrow \infty$ . Integrating over the  $\delta$ -function we obtain

$$\langle \boldsymbol{\varepsilon}\boldsymbol{\varepsilon}^\top \rangle = \int_0^\infty dy \exp(Ly) C \exp(Ly)$$

This matrix-valued integral cannot be evaluated directly, but we can integrate by parts to obtain

$$\begin{aligned} \langle \boldsymbol{\varepsilon}\boldsymbol{\varepsilon}^\top \rangle &= E = \int_0^\infty dy \exp(Ly) C \exp(Ly) \\ &= [\exp(Ly) C \exp(Ly)]_0^\infty L^\dagger - L \int_0^\infty dy \exp(Ly) C \exp(Ly) L^\dagger \\ &= -CL^\dagger - LEL^\dagger \\ \Rightarrow LE + EL &= -C. \end{aligned} \quad (\text{S10})$$

Equation (S10) is the continuous Lyapunov equation, which frequently occurs in control and stability theory [50]. For instance, a linear time-invariant system given by the matrix-valued ODE  $A\dot{\mathbf{x}} = \mathbf{x}$  is globally asymptotically stable if the Lyapunov equation  $A^\top P + PA = -Q$  can be solved for any positive-definite  $Q$ . Here, the dagger represents the Moore-Penrose pseudo-inverse, which is used because the nullspace of  $L$  and  $C$  is given by the vector  $\mathbf{1}$  of all ones. The solution  $E$  must also have  $E\mathbf{1} = 0$  in the centered frame, such that Eq. (S10) captures it fully.

## VI. THE ORDER-PARAMETER HESSIAN NEAR THE SYNCHRONOUS STATE

The Hessian of the squared order parameter for a network of  $N$  oscillators near the fixed point  $\bar{\theta}_j$  is the  $N \times N$  matrix with elements

$$H_{ij} = \frac{2}{N^2} \left( \cos(\bar{\theta}_i - \bar{\theta}_j) - \delta_{ij} \sum_{n=1}^N \cos(\bar{\theta}_i - \bar{\theta}_n) \right).$$

### A. The synchronous state

At the synchronous state  $\bar{\theta}_i = 0$ , the Hessian has the form

$$H_{ij}^{(0)} = \begin{cases} 1 - N & i = j \\ 1 & \text{otherwise.} \end{cases}$$

It is easy to see that the vector of all ones lies in the nullspace,  $H\mathbf{1} = 0$ . Similarly, the set of  $N - 1$  vectors  $(1, -1, 0, \dots, 0), (1, 0, -1, 0, \dots, 0), \dots, (1, 0, \dots, 0, -1)$  provides a basis of the remaining eigenspace corresponding to the eigenvalue  $-2/N$ . Thus, the Hessian is negative semi-definite. We can approximate the eigenvalues for not perfectly synchronized states using perturbation theory. We first note that  $H\mathbf{1} = 0$  is always true due to the structure of the matrix. We then expand the cosines to find the first order correction of  $H = H^{(0)} + H^{(1)} + \dots$  as

$$H_{ij}^{(1)} = -\frac{1}{N^2} \left( (\bar{\theta}_i - \bar{\theta}_j)^2 - \delta_{ij} \sum_{n=1}^N (\bar{\theta}_i - \bar{\theta}_n)^2 \right)$$

It is easy to check that this matrix is negative semi-definite,

$$\sum_{i,j} x_i H_{ij}^{(1)} x_j = -\frac{1}{2N} \sum_{i,j} (\bar{\theta}_i - \bar{\theta}_j)^2 (x_i - x_j)^2 \leq 0.$$

Thus, the eigenspace of  $H^{(0)}$  corresponding to the eigenvalue  $-2/N$  is perturbed to first order to  $-2/N + \lambda_i$ , where  $\lambda_i$  are the eigenvalues of  $H^{(1)}$ . We conclude that close to the synchronous state, the order parameter Hessian  $H$  is negative semi-definite.

### B. Twisted states in periodic chains

Here, we analyze periodic chains of  $N$  oscillators near stable “twisted states.” Following Ref. [49], twisted states are defined by  $\bar{\theta}_j = 2\pi \frac{q}{N} j$ , where  $q = 1, 2, \dots, N - 1$  is the winding number.

The Hessian at a twisted state is

$$H_{ij}^{(0)} = \frac{2}{N^2} \cos \left( 2\pi \frac{q}{N} (i - j) \right),$$

because the sum  $\sum_n \cos(2\pi \frac{q}{N} (i - n)) = 0$ . This matrix is circulant, so the eigenvalues are given by

$$\begin{aligned} \lambda_j &= \sum_{k=1}^N \frac{2}{N^2} \cos \left( 2\pi \frac{q}{N} (k - 1) \right) e^{2\pi i \frac{k-1}{N} j}, \quad j = 0, \dots, N - 1 \\ &= \frac{1}{N^2} \sum_{k=0}^{N-1} \left[ \left( e^{2\pi i \frac{j+k}{N} q} \right)^k + \left( e^{2\pi i \frac{j-k}{N} q} \right)^k \right] \\ &= \begin{cases} \frac{1}{N} & j = q \\ \frac{1}{N} & j = N - q \\ 0 & \text{otherwise.} \end{cases} \end{aligned}$$

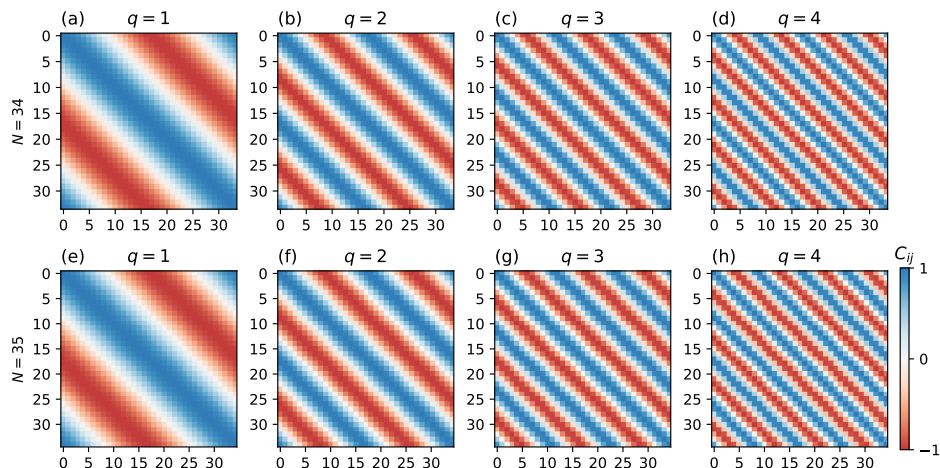


FIG. S2. Optimal noise covariances for twisted states with  $q = 1, 2, 3, 4$  in periodic chains. (a–d) Chains of length  $N = 34$ . (e–h) Chains of length  $N = 35$ . In both cases, the optimal noise pattern is oscillatory with a wavelength that decreases with the winding number  $q$ .

Thus, the Hessian at a twisted state fixed point is positive semi-definite. Expanding near a twisted state,  $\bar{\theta}_j = 2\pi qj/N + \epsilon_j$  the lowest order correction to the Hessian can be written as

$$H_{ij}^{(1)} = -\sin\left(2\pi\frac{q}{N}(i-j)\right)(\epsilon_i - \epsilon_j) + \delta_{ij} \sum_n \sin\left(2\pi\frac{q}{N}(i-n)\right)(\epsilon_i - \epsilon_n).$$

This matrix is indefinite in general, such that the full Hessian eigenvalues close to twisted states are generally indefinite. Numerically it can be seen that near a twisted state, the 0-eigenvalues of  $H^{(0)}$  tend to split into positive and negative pairs of eigenvalues.

## VII. OPTIMAL NOISE FOR TWISTED STATES IN PERIODIC CHAINS

Here, we analyze periodic chains of  $N$  oscillators near stable “twisted states.” Following Ref. [49], we set  $\omega_i = 0$  and choose twisted initial conditions,  $\bar{\theta}_j = 2\pi\frac{q}{N}j$ , where  $q = 1, 2, \dots, N-1$  is the winding number. Such twisted states can be thought of as maximally asynchronous because the order parameter is

$$R = \frac{1}{N} \sum_{j=1}^N e^{2\pi i \frac{q}{N} j} = 0.$$

Thus, near stable twisted states we expect any amount of noise to increase the order parameter. Specifically, we find that our method as outlined in the main paper still works and provides optimal noise patterns which improve  $\langle R^2 \rangle$  compared to uncorrelated noise and to the no-noise case.

The optimal noise covariances are no longer anticorrelated between neighboring oscillators but oscillate spatially with a wavelength that decreases with increasing winding number  $q$  (Figure S2).

Direct numerical simulations show that optimal noise patterns do improve synchrony as compared to uniform noise (Figure S3). Because for higher winding numbers  $q$  the basins of attraction of the twisted states become smaller, it becomes steadily more difficult to remain near the twisted state in a noisy system. For instance, in the  $N = 10$  chain from Figure S3, states with  $q > 2$  were not stable for any amount of noise  $\sigma > 10^{-6}$ .

## VIII. OPTIMAL NOISE IN PERIODIC SQUARE GRIDS

Periodic grids show similar behavior as oscillator chains. In a periodic even square grid, the optimal noise is perfectly anti-correlated between neighboring nodes [Fig. S4 (a,b)], whereas for odd square grids, correlations show a characteristic decay similar to odd chains due to the fact that not all neighbors can receive perfectly anti-correlated inputs [Fig. S4 (c,d)].



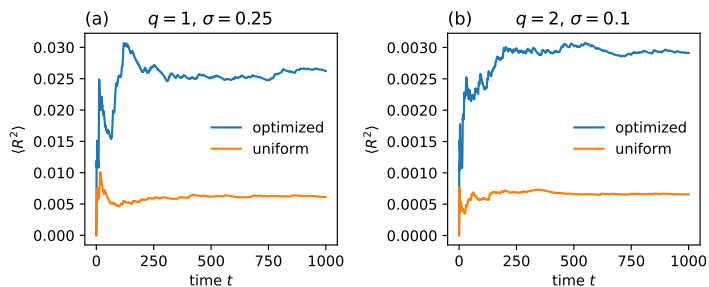


FIG. S3. Time series of the time averaged order parameter  $\langle R^2 \rangle(t) = (1/t) \int_0^t R^2(t') dt'$  in an  $N = 10$  periodic chain near twisted states with winding numbers (a)  $q = 1$  and (b)  $q = 2$ . For panel (a),  $\sigma = 0.25$  and for panel (b),  $\sigma = 0.1$ .

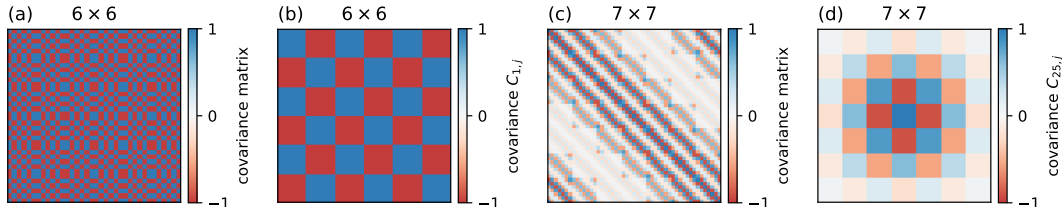


FIG. S4. Optimal noise patterns and frustrated covariances in periodic square grids. (a) Optimal covariance matrix of a  $6 \times 6$  periodic square grid of oscillators. (b) Covariance pattern for the same grid as in panel (a) with respect to the top left oscillator, all neighbors are anti-correlated. Each matrix entry corresponds to one oscillator in the grid with neighbors as shown. (c) Optimal covariance matrix of a frustrated  $7 \times 7$  periodic square grid of oscillators. Because the graph has an odd number of oscillators in each direction, not all neighbors can receive anti-correlated noise. (d) Covariance pattern for the same grid as in panel (c) with respect to the center oscillator. Covariances decay with distance, similar to Fig. 2 (d,f).

## IX. PARAMETRIC DEPENDENCE OF THE OPTIMAL COVARIANCE IN PERIODIC CHAINS AND OPTIMAL NOISE TRANSITION

In the following section we study the dependence of the optimal noise covariance matrix on the parameters of the system, the coupling constant  $K$  and the distribution of natural frequencies  $\omega_i$ . For simplicity, we focus on periodic oscillator chains and on Gaussian distributed natural frequencies with zero mean where we vary the width of the distribution. For couplings  $K$  close to the synchronization transition, a new transition in the optimal noise covariances is observed from small-scale to large-scale correlations. The width of the transition region depends on the width of the distribution of natural frequencies. The optimal noise covariance matrix obtained close to the synchronization transition in the phase-locked regime still provides a significant improvement in the order parameter even in the phase-drift regime, for a large range of parameters even beyond the noise-free order parameter.

### A. Dependence on the coupling constant and noise strength

Here we study the dependence of the optimal covariance matrix on the coupling  $K$  in periodic chains. We fixed chains of length  $N = 11, 12$  as in the main paper with random but fixed distribution of natural frequencies  $\{\omega_i\}$  where the standard deviation was  $\text{std}(\{\omega_i\}) = 1/N$ . We varied the uniform coupling constant  $K$  between  $K = 0$  and  $K = 1$ .

We numerically integrated the stochastic equations of motion from initial conditions at the steady state if one existed (computed as in Section IV) or from zero initial conditions (if no steady state existed) for (i) no noise, (ii) uncorrelated noise, and (iii) optimal noise. When a steady state existed at a given  $K$ , the optimal noise was obtained using the same method as described in the main paper. When no steady state existed at a given  $K$ , the optimal noise from the closest  $K$  where a steady state existed was used. The noise variance was fixed to  $\sigma = 0.5$  and the equations of motion were integrated until  $t = 200000$ .

Generally, we found that in the steady-state regime the behavior was as expected from the main paper (Figure S5). Specifically, it is possible that the choice of natural frequencies  $\omega_i$  is such that close to the synchronization transition, the optimal noise also undergoes a transition and becomes significantly better at synchronizing the network than even the no-noise case [Fig. S5 (a,c)]. The transition of the optimal noise covariance matrix depends on the network topology

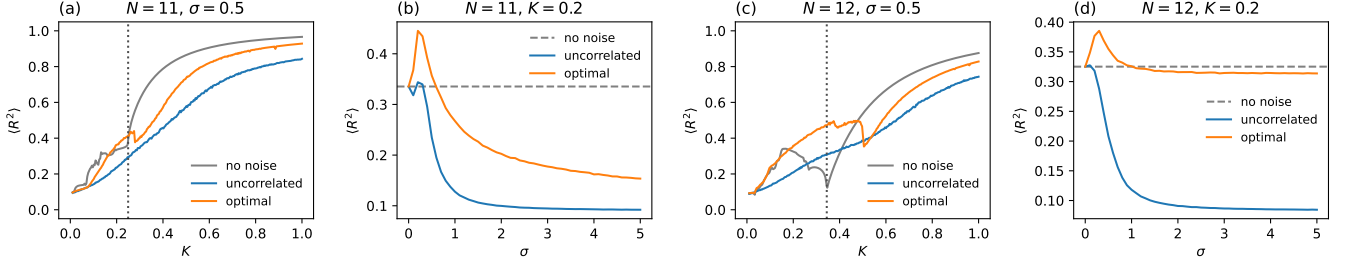


FIG. S5. Dependence of the long-time averaged order parameter  $\langle R^2 \rangle$  on the parameters  $K$  and  $\sigma$  in periodic chains of (a,b)  $N = 11$  and (c,d)  $N = 12$ . Panels (a,c) show the order parameter without noise (from direct numerical simulations and from theory by numerically calculating the fixed point), with optimal noise, and with uncorrelated noise of equal total variance. The optimal noise covariance matrix  $C$  was calculated for each value of  $K$  independently. In the phase-drift regime, the matrix  $C$  corresponding to the closest value of  $K$  where a fixed point existed was used. The vertical dotted lines correspond to the critical values  $K_{\text{crit}}$  where the synchronization transition occurred. Numerical simulation were performed from initial conditions either at the numerically obtained noise-free fixed point (in the phase-locked regime) or from zero initial conditions (in the phase-drift regime) up to a time  $t = 200000$ .

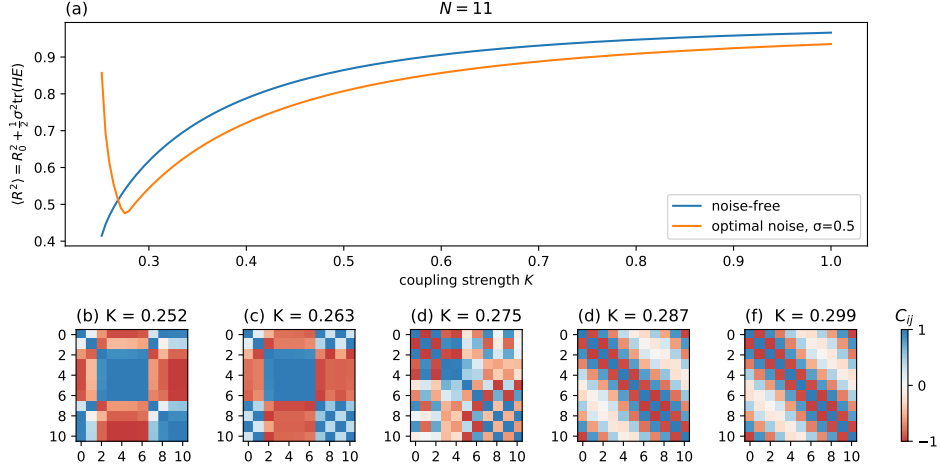


FIG. S6. Optimal noise covariances near the synchronization transition in an  $N = 11$  chain. (a) Noise-free and approximate optimal noise order parameters as a function of the coupling strength  $K$ . The optimal noise curve crosses the no-noise curve near the synchronization transition. The curves correspond to those in Fig. S5 (a). (b–e) Optimal covariance matrices near the synchronization transition, exhibiting a transition from small scale to large scale correlations.

and proceeds towards more large-scale correlations as the synchronization transition is approached (Figures S6, S7).

## B. Dependence on the frequency distribution

To study the dependence on the frequency distribution, we again consider periodic chains of various sizes. For simplicity, we consider only Gaussian distributed natural frequencies  $\omega_i$ , but we vary the the standard deviation,  $\text{std}(\omega)$ . We choose periodic oscillator chains of sizes  $N = 10, 12, 15$  and perform numerical optimizations of the noise covariances. For each oscillator chain, the distribution of  $\omega_i$ 's is fixed and then the initial distribution is uniformly rescaled to obtain different standard deviations.

In all cases, we find the same transition if the optimal noise covariance near the synchronization transition of the original system. However, the transition happens over a smaller range of  $K$  as the standard deviation  $\text{std}(\omega)$  is decreased (Figure S8).

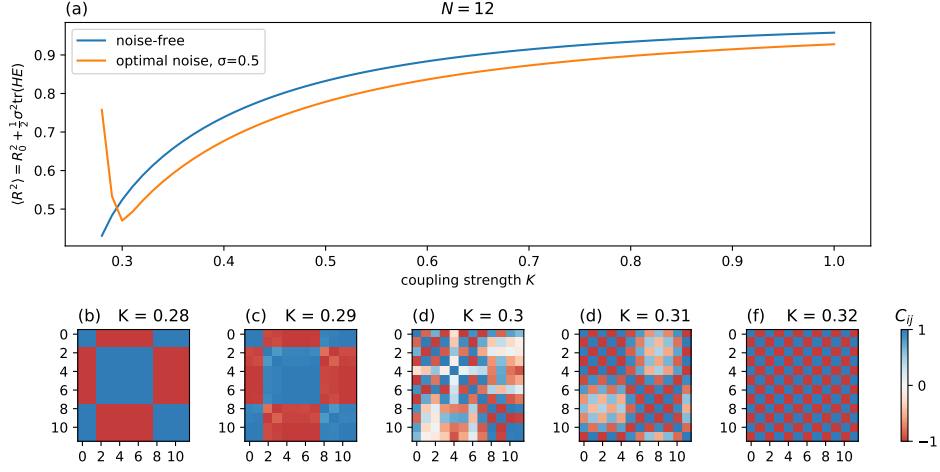


FIG. S7. Optimal noise covariances near the synchronization transition in an  $N = 12$  chain. (a) Noise-free and approximate optimal noise order parameters as a function of the coupling strength  $K$ . The optimal noise curve crosses the no-noise curve near the synchronization transition. The curves correspond to those in Fig. S5 (c). (b–e) Optimal covariance matrices near the synchronization transition, exhibiting a transition from small scale to large scale correlations.

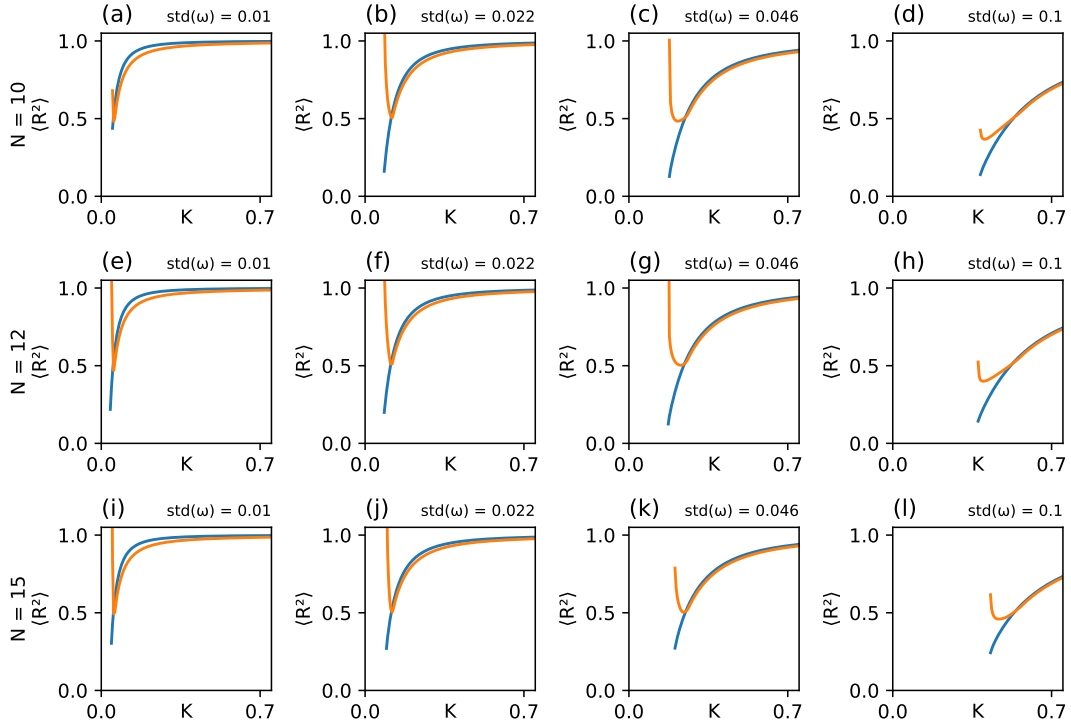


FIG. S8. Dependence of the optimal noise transition on the frequency distribution. (a–c)  $N = 10$  periodic chain, (e–f)  $N = 12$  periodic chain, (i–l)  $N = 15$  periodic chain. Shown are the steady-state order parameters  $R_0^2$  without noise (blue lines) and the approximations  $\langle R^2 \rangle = R_0^2 + (\sigma^2/2) \text{tr}(HE)$  with  $\sigma = 0.25$  (orange lines). The synchronization transition where steady states cease to exist occurs at the value of  $K$  where both lines end.

## X. SECOND-ORDER POWER GRID MODELS

Power grids are often modeled using the swing equation (a second-order Kuramoto model), which includes the effects of mechanical inertia in the grid [9]. The equations of motion for  $N$  nodes are

$$\begin{aligned}\dot{\theta}_i &= \omega_i \\ \dot{\omega}_i &= -\alpha \omega_i + \sum_{j=1}^N K_{ij} \sin(\theta_j - \theta_i) + P_i + \eta_i.\end{aligned}\tag{S11}$$

Here,  $\alpha$  is a damping constant,  $K_{ij}$  are coupling constants related to physical properties of the grid power lines, and the constants  $P_i$  are related to net power flows (generation or consumption) at each node  $i$ . The  $\eta_i$  are noise terms with  $\langle \eta_i \rangle = 0$  and  $\langle \eta_i(t) \eta_j(t') \rangle = C_{ij} \delta(t - t')$ . We will also assume that the net powers are balanced,  $\sum_j P_j = 0$ .

Just like in the main manuscript, we can find a noise-free steady state by solving

$$0 = \sum_{j=1}^N K_{ij} \sin(\bar{\theta}_j - \bar{\theta}_i) + P_i,$$

which has the same mathematical form as the equivalent equation in the Kuramoto model. Expanding near this state as  $\theta_i(t) = \bar{\theta}_i + \varepsilon_i(t)$  for small  $\varepsilon_i$  we obtain the linearized equations of motion

$$\underbrace{\begin{pmatrix} \dot{\varepsilon} \\ \dot{\omega} \end{pmatrix}}_{=\dot{\mathbf{y}}} = \underbrace{\begin{pmatrix} 0 & \mathbb{1} \\ L & -\alpha \mathbb{1} \end{pmatrix}}_{=M} \underbrace{\begin{pmatrix} \varepsilon \\ \omega \end{pmatrix}}_{=\mathbf{y}} + \begin{pmatrix} 0 \\ \boldsymbol{\eta}(t) \end{pmatrix}.$$

Here, we again used the Laplacian with components  $L_{ij} = K_{ij} \cos(\bar{\theta}_j - \bar{\theta}_i) - \delta_{ij} \sum_n K_{in} \cos(\bar{\theta}_n - \bar{\theta}_i)$ . For this linearized system, we can go through the same derivation as in Section V to show that the long-time covariance matrix  $F = \langle \mathbf{y} \mathbf{y}^\top \rangle$  satisfies another Lyapunov equation,

$$MF + FM^\top = -\begin{pmatrix} 0 & 0 \\ 0 & C \end{pmatrix} = -\hat{C}.$$

Note the transpose ‘ $\top$ ’, which is due to the fact that  $M$  is not symmetric.

The synchrony of a power grid can be quantified by the same type of long-time averaged order parameter as in the Kuramoto model,

$$\begin{aligned}\langle R^2 \rangle &= R_0^2 + \frac{1}{2} \langle \boldsymbol{\varepsilon}^\top H \boldsymbol{\varepsilon} \rangle + \dots \\ &= R_0^2 + \frac{1}{2} \text{tr}(HE) + \dots\end{aligned}$$

Here,  $H$  is the same Hessian as in the main paper and the matrix  $E$  of covariances between the  $\boldsymbol{\varepsilon}$ ’s is the top left  $N \times N$  block of

$$F = \begin{pmatrix} E & * \\ * & * \end{pmatrix}.$$

Armed with this model, we can formulate the optimal noise problem for power grids as

$$\begin{aligned}\max_{C, F} \quad & \text{tr}(HE) \\ \text{such that} \quad & MF + FM^\top = -\hat{C} \\ & C \succeq 0.\end{aligned}\tag{S12}$$

We numerically optimized the IEEE 14-bus test case near its synchronous steady state for various values of  $\alpha$  (Fig. S9). For large  $\alpha \gg 1$ , the model approaches the Kuramoto case, and the optimal covariances are clustered. Decreasing  $\alpha$ , and thus increasing the relative importance of inertia, the optimal covariances become less clustered by going through a number of step-like transitions in the covariance structure. At the same time, the optimal objective  $\text{tr}(HE)$  decreases: in strongly inertia-dominated networks, noise optimization is less effective at increasing synchrony. However, the basic anti-correlated structure of optimal covariances remains.

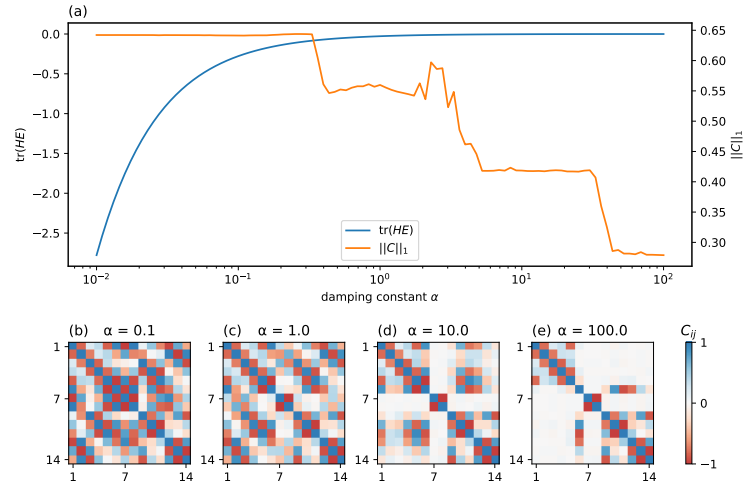


FIG. S9. Optimal noise covariance matrices  $C$  in the IEEE 14-bus test grid with the swing equation model Eq. (S12). (a) We plot the optimal value of the objective function  $\text{tr}(HE)$  against the damping parameter  $\alpha$ , and we quantify the structure of the optimal covariance matrix using its Frobenius 1-norm  $\|C\|_1 = \sum_{i,j} |C_{ij}|$ , revealing a number of transitions (b–e).